Available online at www.sciencedirect.com

ScienceDirect

IFAC PapersOnline CONFERENCE PAPER ARCHIVE

IFAC PapersOnLine 53-2 (2020) 7248–7255

Global Sensitivity Methods for Design of Experiments in Lithium-ion Battery Context ⋆

A. Pozzi ** **X. Xie*** **D.M. Raimondo** ** **R. Schenkendorf***

* *Institute of Energy and Process Systems Engineering, TU Braunschweig, 38106 Braunschweig, Germany (e-mail: {x.xie,r.schenkendorf}@tu-braunschweig.de)*

** *Department of Electrical, Computer and Biomedical Engineering, University of Pavia, 27100 Pavia, Italy (e-mail: andrea.pozzi03@universitadipavia.it, davide.raimondo@unipv.it)*

Abstract: Battery management systems may rely on mathematical models to provide higher performance than standard charging protocols. Electrochemical models allow us to capture the phenomena occurring inside a lithium-ion cell and therefore, could be the best model choice. However, to be of practical value, they require reliable model parameters. Uncertainty quantification and optimal experimental design concepts are essential tools for identifying systems and estimating parameters precisely. Approximation errors in uncertainty quantification result in sub-optimal experimental designs and consequently, less-informative data, and higher parameter unreliability. In this work, we propose a highly efficient design of experiment method based on global parameter sensitivities. This novel concept is applied to the single-particle model with electrolyte and thermal dynamics (SPMeT), a well-known electrochemical model for lithium-ion cells. The proposed method avoids the simplifying assumption of output-parameter linearization (i.e., local parameter sensitivities) used in conventional Fisher information matrix-based experimental design strategies. Thus, the optimized current input profile results in experimental data of higher information content and in turn, in more precise parameter estimates.

Keywords: parameter identification, global parameter sensitivities, uncertainty quantification, design of experiments, lithium-ion batteries.

1. INTRODUCTION

In the field of lithium-ion batteries, first-principle models have proven to be beneficial in providing battery management systems with high performance and high safety standards (Chaturvedi et al., 2010). First-principle models are used in general to gain physical insights, monitor, and control complex processes. For models to be reliable, high accuracy, in terms of structure and parameters, is required. In practice, model structures are approximated based on simplifying assumptions that aim to guarantee identifiability while retaining a physical interpretation. Unfortunately, the possible imprecision of the structure, together with the fact that model parameters are obtained in general using noisy measurement data, may result in uncertain parameter estimates and inaccurate simulation results (Walter and Pronzato, 1997). To alleviate these issues, the use of accurate uncertainty quantification in combination with a model-based design of experiment (MBDoE) can provide an improved model calibration with more reliable parameter estimates. In particular, the MBDoE consists of finding the optimal input sequence able to minimize the uncertainty of the model parameters (Pukelsheim, 2006).

Most implementations of MBDoE are based on the Fisher information matrix (FIM), which gives a local measurement of how informative a measured signal is in terms of parameter sensitivity. In particular, the FIM represents a perfect MBDoE measure only for linear parameter identification problems (Kiefer, 1959; Walter and Pronzato, 1997; Sinkoe and Hahn, 2017). Local parameter sensitivities assume a linear relationship between model parameter variations and simulation results. In the nonlinear case, local sensitivities may lead to biased local parameter sensitivity and MBDoE measures because of biased reference parameters (Manesso et al., 2017). Moreover, the actual parameter values for calculating these local parameter sensitivities are unknown, and, in turn, the best parameter estimates have to be used.

In the last decade, the use of global sensitivities for the MBDoE has been discussed in the literature (Rodriguez-Fernandez et al., 2007; Chu and Hahn, 2013; Schenkendorf et al., 2018). Global parameter sensitivities, by definition, represent nonlinear and multivariate parameter dependencies adequately. Global parameter sensitivities

⋆ X. Xie acknowledges support from the International Max Planck Research School for Advanced Methods in Process and Systems Engineering, MPI Magdeburg. D.M. Raimondo has been (partially) supported by the Italian Ministry for Research in the framework of the 2017 Program for Research Projects of National Interest (PRIN), Grant no. 2017YKXYXJ.

10.1016/j.ifacol.2020.12.558

consider model parameters and simulation results as random variables. Thus, the global sensitivity analysis (GSA) aims to quantify the amount of variation that each model parameter contributes to the variation in the simulation results.

Most lithium-ion cell models employed in advanced battery management systems (BMSs) can be grouped into two main categories: equivalent circuit models (ECMs; Hu et al. (2012)), which are intuitive and straightforward, and electrochemical models (EMs; Gomadam et al. (2002); Santhanagopalan et al. (2006)), which are far more accurate. The pseudo-two-dimensional (P2D) model (Doyle et al., 1993), which consists of nonlinear partial differential algebraic equations (PDAEs), is the most widely used EM. However, the use of the latter for control purposes is limited due to its high computational burden and its identifiability and observability issues (Forman et al., 2012; Moura, 2015). The aforementioned issues can be addressed by reduced order models, which have raised the interest of the research community, due to the fact that they still provide a sufficiently detailed description of the electrochemical phenomena (Zou et al., 2014). Parameter identifiability and state observability of the single particle model (SPM; Ning and Popov (2004); Santhanagopalan et al. (2006)), which models the electrodes as single particles, have been analyzed in several works (Di Domenico et al., 2010; Bizeray et al., 2018; Pozzi et al., 2018a). The electrolyte (SPMe; Moura et al. (2017)) and thermal dynamics (SPMeT; Perez et al. (2016)) can also be considered in order to increase the model accuracy. In the literature, various MBDoE studies exist, including ones for complex (electro)chemical processes. For instance, the usefulness of MBDoE for lithium-ion battery models (both full and reduced-order ones) was demonstrated recently in Mendoza et al. (2016, 2017); Pozzi et al. (2018b); Park et al. (2018b,a), where the current profile is optimized by relying on the FIM to maximize the identifiability of the parameters.

To the best of the authors' knowledge, the usefulness of GSA and its effective implementation for (electro)chemical processes in the context of MBDoE have not been analyzed thus far. In this work, we propose a highly efficient MBDoE framework that is based on GSA, and we implement this novel GSA-MBDoE concept for a lithium-ion cell modelled as SPMeT. It has to be noticed that the proposed concept avoids the simplifying assumption of output-parameter linearization used in standard MBDoE strategies. To prevent a computation overload while replacing the local parameter sensitivity matrix and solving the underlying dynamic optimization problem, we make use of the point estimate method (PEM) as a highly efficient sampling technique to determine global parameter sensitivities. In contrast to previous work (Schenkendorf et al., 2018), the global parameter sensitivities are directly transferred to standard DoE criteria.

The paper is organized as follows. In Section 2, the SPMeT is introduced, including modeling assumptions and governing equations. In Section 3, the basic concepts of the model-based design of experiments are summarized, and the novel experimental design, which is based on global parameter sensitivities, is proposed. In Section 4, the standard MBDoE approach and the novel GSA-MBDoE concepts are applied to the lithium-ion battery model and critically compared. Finally, in Section 5, the results are summarized and conclusions provided.

2. LITHIUM-ION BATTERY MODEL

In this study, we consider the single-particle model with electrolyte and thermal dynamics, which has proven to be accurate enough but also suitable for real-time implementation in advanced battery management systems (Moura et al., 2017). In the following, the cell sections are indexed with $j \in \{p, s, n\}$ in all the equations except for those valid only for the electrodes where the index i refers to $\{p, n\}$ instead. The variables $t \in \mathbf{R}$, $x \in \mathbf{R}$ and $r \in \mathbf{R}$ indicate respectively the time index, the spatial direction along which the lithium ions are transported and the radial distance within an active particle at location x. As previously done in this context by Subramanian et al. (2005), a fourth-order polynomial approximation of the ion concentration along the radial axis r of each electrode is considered. In particular, the concentration is described as a function of r, whose coefficients depend on the solid average concentration $\bar{c}_{s,i}(t)$ and the average concentration flux $\bar{q}_i(t)$. Let the average stoichiometry in the electrodes be defined by:

$$\bar{\theta}_i(t) = \frac{\bar{c}_{s,i}(t)}{c_{s,i}^{max}}, \tag{1}$$

where $c_{s,i}^{max}$ is the maximum solid concentration. The dynamics of the average stoichiometries can be expressed by the following equation (Subramanian et al., 2005):

$$\dot{\bar{\theta}}_i(t) = \frac{3I_{app}(t)}{a_i R_{p,i} L_i F A c_{s,p}^{max}}, \tag{2}$$

where the thickness of the ith section is described by L_i, the particle radius is denoted by $R_{p,i}$, F is the Faraday constant, A is the area of the cell, $I_{app}(t)$ is the input current (with the assumption that a negative current charges the cell) and $a_i = \frac{3\epsilon_i^{act}}{R_{p,i}}$ is the specific active surface area, with ϵ_i^{act} the active material volume fraction defined by:

$$\epsilon_p^{act} = -\frac{C}{\Delta\theta_p A F L_p c_{s,p}^{max}}, \tag{3a}$$

$$\epsilon_n^{act} = \frac{C}{\Delta\theta_n A F L_n c_{s,n}^{max}}, \tag{3b}$$

in which the cell capacity is represented by C. Considering $\theta_i^{0\%}$ and $\theta_i^{100\%}$ the stoichiometries of the electrodes in the case of fully discharged and fully charged cell respectively, it holds that $\Delta\theta_i = \theta_i^{100\%} - \theta_i^{0\%}$. The concentration fluxes present the following dynamics:

$$\dot{\bar{q}}_p(t) = -30\frac{D_{s,p}(T(t))}{R_{p,p}^2}\bar{q}_p(t) + \frac{45}{2R_{p,p}^2 F A L_p a_p} I_{app}(t), \tag{4a}$$

$$\dot{\bar{q}}_n(t) = -30\frac{D_{s,n}(T(t))}{R_{p,n}^2}\bar{q}_n(t) - \frac{45}{2R_{p,n}^2 F A L_n a_n} I_{app}(t), \tag{4b}$$

where $T(t)$ is the temperature, and $D_{s,i}(T(t))$ is the solid diffusion coefficient for the ith section, which depends on the temperature according to the Arrhenius law. Considering the assumption of lithium moles conservation in

the solid phase (Di Domenico et al., 2010), the average stoichiometry in the anode can be obtained directly from the cathode as follows:

$$\bar{\theta}_n(t) = \theta_n^{0\%} + \frac{\bar{\theta}_p(t) - \theta_p^{0\%}}{\theta_p^{100\%} - \theta_p^{0\%}}(\theta_n^{100\%} - \theta_n^{0\%}). \tag{5}$$

In this way, $\bar{\theta}_n(t)$ can be considered as an output of the system, thus reducing the number of state equations and increasing the computational efficiency.

The surface stoichiometries in the electrodes can be computed with the following algebraic equations:

$$\theta_p(t) = \bar{\theta}_p(t) + \frac{8R_{p,p}\bar{q}_p(t)}{35c_{s,p}^{max}} + \frac{R_{p,p}I_{app}(t)}{35D_{s,p}(T(t))FAL_p a_p c_{s,p}^{max}}, \tag{6a}$$

$$\theta_n(t) = \bar{\theta}_n(t) + \frac{8R_{p,n}\bar{q}_n(t)}{35c_{s,n}^{max}} - \frac{R_{p,n}I_{app}(t)}{35D_{s,n}(T(t))FAL_n a_n c_{s,n}^{max}}, \tag{6b}$$

according to the polynomial approximation of the lithium concentration along the radius of the particle (Subramanian et al., 2005).

The state of charge (SOC) is defined as:

$$SOC(t) = 100\frac{\bar{\theta}_n(t) - \theta_n^{0\%}}{\theta_n^{100\%} - \theta_n^{0\%}}. \tag{7}$$

A fundamental output of the SPMeT is the terminal voltage $V(t)$. This latter not only depends on the lithium concentration in the solid phase but also on the one in the electrolyte. Therefore, the PDAEs governing the diffusion of the electrolyte concentration $c_{e,j}(x,t)$ must be considered. In this work, the finite volume method is exploited for spatially discretizing such PDAEs, as previously done in this context by Torchio et al. (2016). The authors in Torchio et al. (2016) divide the spatial domain into P non-overlapping volumes for each section. For each section j, each volume ranges within $\Omega_{j,k} = \left[x_{j,\underline{k}}, x_{j,\bar{k}}\right]$, with $k = 1, \cdots, P$, with center $x_{j,k}$ and width $\Delta x_j = L_j/P$. Defining $c_{e,j}^{[k]}(t)$ as the average electrolyte concentration over the kth volume of the jth section gives:

$$\epsilon_p \frac{\partial c_{e,p}^{[k]}(t)}{\partial t} = \left[\frac{\tilde{D}_e(x,T(t))}{\Delta x_p}\frac{\partial c_{e,p}(x,t)}{\partial x}\right]\Bigg|_{x_{p,\underline{k}}}^{x_{p,\bar{k}}} - \frac{1-t_+}{FAL_p}I_{app}(t), \tag{8a}$$

$$\epsilon_s \frac{\partial c_{e,s}^{[k]}(t)}{\partial t} = \left[\frac{\tilde{D}_e(x,T(t))}{\Delta x_s}\frac{\partial c_{e,s}(x,t)}{\partial x}\right]\Bigg|_{x_{s,\underline{k}}}^{x_{s,\bar{k}}}, \tag{8b}$$

$$\epsilon_n \frac{\partial c_{e,n}^{[k]}(t)}{\partial t} = \left[\frac{\tilde{D}_e(x,T(t))}{\Delta x_n}\frac{\partial c_{e,n}(x,t)}{\partial x}\right]\Bigg|_{x_{n,\underline{k}}}^{x_{n,\bar{k}}} + \frac{1-t_+}{FAL_n}I_{app}(t), \tag{8c}$$

where t_+ is the transference number, ϵ_j is the material porosity, and $\tilde{D}_e(x,T(t))$ is the electrolyte diffusion coefficient which is computed according to the harmonic mean. See Torchio et al. (2016) for a further description of the terms in the electrolyte dynamics. Note that the effective diffusion and conductivity coefficients are according to the Bruggeman's theory, where τ_j represents the tortuosity factor for each section.

The dependence on the temperature of the parameters above is described by the Arrhenius law, which, for a generic parameter $\psi(T(t))$, is given by:

$$\psi(T(t)) = \psi^0 e^{-\frac{E_{a,\psi}}{RT(t)}}, \tag{9}$$

where ψ^0 and $E_{a,\psi}$ are the constant coefficient and the activation energy related to the parameter $\psi(T(t))$, and R is the universal gas constant.

The terminal voltage is then given by:

$$\begin{aligned} V(t) = &- I_{app}(t)R_{sei} + \bar{U}_p(t) - \bar{U}_n(t) + \bar{\eta}_p(t) - \bar{\eta}_n(t) \\ &+ \Delta\Phi_e(t), \end{aligned} \tag{10}$$

where R_{sei} is the solid electrolyte interface (SEI) resistance, while $\bar{U}_p(t)$ and $\bar{U}_n(t)$ are the Open Circuit Potentials (OCPs) in the positive and negative electrodes. The overpotentials $\bar{\eta}_p(t)$ and $\bar{\eta}_n(t)$, for the positive and negative electrodes are given respectively by:

$$\bar{\eta}_p(t) = \frac{2RT(t)}{F}\sinh^{-1}\left(\frac{-I_{app}(t)}{2AL_p a_p \bar{i}_{0,p}(t)}\right), \tag{11a}$$

$$\bar{\eta}_n(t) = \frac{2RT(t)}{F}\sinh^{-1}\left(\frac{I_{app}(t)}{2AL_n a_n \bar{i}_{0,n}(t)}\right). \tag{11b}$$

The exchange current density is defined as:

$$\bar{i}_{0,i}(t) = Fk_i(T(t))\sqrt{\bar{c}_{e,i}(t)\theta_i(t)(1-\theta_i(t))}, \tag{12}$$

where $k_i(T(t))$ is the temperature-dependent rate reaction coefficient and $\bar{c}_{e,i}(t)$ is obtained by averaging the electrolyte concentration over the ith section concentration as follows:

$$\bar{c}_{e,i}(t) = \frac{1}{P}\sum_{k=1}^{P} c_{e,i}^{[k]}(t). \tag{13}$$

Moreover, $\Delta\Phi_e(t)$ is computed as:

$$\Delta\Phi_e(t) = \Phi_e^{drop}(t) + \frac{2RT}{F}(1-t_+)\log_e\left(\frac{c_{e,p}^{[1]}}{c_{e,n}^{[P]}}\right), \tag{14}$$

where the shape of the ionic current $i_e(x,t)$ is assumed to be trapezoidal over the spatial domain (Moura et al., 2017). The electrolyte voltage drop $\Phi_e^{drop}(t)$ can be approximated by:

$$\Phi_e^{drop}(t) \simeq -\frac{I_{app}(t)}{2A}\left(\phi_p(t) + 2\phi_s(t) + \phi_n(t)\right), \tag{15}$$

in which:

$$\phi_p(t) = \Delta x_p \sum_{k=1}^{P}\frac{2k-1}{\kappa(c_{e,p}^{[k]}(t))\epsilon_p^{p_p}}, \tag{16a}$$

$$\phi_s(t) = \Delta x_s \sum_{k=1}^{P}\frac{1}{\kappa(c_{e,s}^{[k]}(t))\epsilon_s^{p_s}}, \tag{16b}$$

$$\phi_n(t) = \Delta x_n \sum_{k=1}^{P}\frac{2P-2k+1}{\kappa(c_{e,n}^{[k]}(t))\epsilon_n^{p_n}}, \tag{16c}$$

where, for the kth volume of the jth section, the electrolyte conductivity is described by $\kappa(c_{e,j}^{[k]}(t))$. This latter that can be derived empirically is expressed with a nonlinear function of the electrolyte concentration:

$$\begin{aligned} \kappa(\gamma_j^{[k]}(t)) = &\Big(0.2667\left(\gamma_j^{[k]}(t)\right)^3 - 1.2983\left(\gamma_j^{[k]}(t)\right)^2 \\ &+ 1.7919\gamma_j^{[k]}(t) + 0.1726\Big)e^{\frac{-E_{a,\kappa}}{RT(t)}}, \end{aligned} \tag{17}$$

where $\gamma_j^{[k]}(t) = 10^{-3} c_{e,j}^{[k]}(t)$. The function in Eq. (17) is taken from Ecker et al. (2015b) as well as the expressions of the OCPs in terms of the surface stoichiometries:

$$\begin{aligned}\bar{U}_p(t) =& 18.45\theta_p^6(t) - 40.7\theta_p^5(t) + 20.94\theta_p^4(t) \\ &+ 8.07\theta_p^3(t) - 7.837\theta_p^2(t) + 0.02414\theta_p^1(t) + 4.571,\end{aligned} \tag{18a}$$

$$\bar{U}_n(t) = \frac{0.1261\theta_n(t) + 0.00694}{\theta_n^2(t) + 0.6995\theta_n(t) + 0.00405}, \tag{18b}$$

which are fitted from experimentally collected data. Note that the empirical functions in Eqs. (17) and (18a) may vary according to the considered cell (in the presented paper, Kokam SLPB 75106100).

Finally, the temperature dynamics is given by a lumped thermal model (Perez et al., 2016, 2017):

$$C_{th}\dot{T}(t) = Q(t) - h_c A_c (T(t) - T_{sink}), \tag{19}$$

where C_{th} is the thermal capacity of the cell, and h_c and A_c are the convective coefficient and the area of the heat exchange with the coolant, respectively. We assume that the coolant temperature is constant and equal to T_{sink}. The heat $Q(t)$ is generated by the cell polarization as follows:

$$Q(t) = |I_{app}(t)| \cdot |V(t) - (\bar{U}_p(t) - \bar{U}_n(t))|. \tag{20}$$

The electrochemical parameters adopted are those measured in Ecker et al. (2015b,a), in which a commercial cell (the Kokam SLPB 75106100) is completely characterized through experiments. The value of the sink temperature is constant and set to $T_{sink} = 298.15\,\mathrm{K}$, while the thermal capacity is set to $C_{th} = 4186\,\mathrm{JK}^{-1}$. Finally, the heat exchange parameters are assumed to be $A_c = 1\,\mathrm{m}^2$ and $h_c = 10\,\mathrm{W\,m^{-2}\,K^{-1}}$.

3. MODEL-BASED DESIGN OF EXPERIMENTS

Next, we propose the GSA-MBDoE concept. The underlying dynamic optimization problem is introduced first. Then, the basics of local and global parameter sensitivities are briefly summarized. The point estimate method is presented to ensure fast GSA-MBDoE results.

3.1 Optimization Framework

In this study, the MBDoE states a dynamic optimization problem and reads as:

$$\max_{\mathbf{u}(\cdot)} \ \Phi(S^{l/g}(\mathbf{p})) \tag{21a}$$

subject to:

$$\dot{\mathbf{x}}_\mathbf{d}(t) = \mathbf{f}(\mathbf{x_d}(t), \mathbf{u}(t), \mathbf{p}), \tag{21b}$$

$$\mathbf{x_d}(t_0) = \mathbf{x}_0, \tag{21c}$$

$$0 \leq \mathbf{h_{nq}}(\mathbf{x_d}(t), \mathbf{u}(t), \mathbf{p}), \tag{21d}$$

$$\mathbf{u}_{min} \leq \mathbf{u} \leq \mathbf{u}_{max}, \tag{21e}$$

where $t \in [t_0, t_0 + t_{exp}]$ is the time, with $t_0 = 0s$ is the initial time and t_{exp} is the time duration of the experiment, $\mathbf{u} \in \mathbf{R}^{n_u}$ is the vector of the control variables, $\mathbf{p} \in \mathbf{R}^{n_p}$ is the vector of the time-invariant parameters, and $\mathbf{x_d} \in \mathbf{R}^{n_{x_d}}$ are the differential states. The initial conditions for the differential states are given by $\mathbf{x}_0$ while $\mathbf{y} \in \mathbf{R}^{n_y}$ is the vector of the model output. Eq. (21b) is the model equation with $\mathbf{f} : \mathbf{R}^{n_{x_d} \times n_u \times n_p} \to \mathbf{R}^{n_{x_d}}$. To satisfy critical process constraints, Eq. (21d) represents the inequality constraints $\mathbf{h_{nq}} : \mathbf{R}^{n_{x_d} \times n_u \times n_p} \to \mathbf{R}^{n_{nq}}$. $[\mathbf{u}_{min}, \mathbf{u}_{max}]$ are the upper and lower boundaries for the control variables. The parameter sensitivity measure $S^{l/g}(\mathbf{p})$ determines the effectiveness of the MBDoE strategy. In this work, local, S^l, and global parameter sensitivities, S^g, are used. The parameter sensitivities are translated to a cost function $\Phi(\cdot)$, where different MBDoE cost functions exist in the literature (Walter and Pronzato, 1997; Pukelsheim, 2006).

Let us consider a sampling time t_s and a positive integer number $K = \frac{t_{exp}}{t_s}$ of discrete time measurements $\mathbf{y}^{\mathrm{data}}(t_k)$, with $t_{k+1} = t_k + t_s$, for $k \in [0, K]$. Assuming a maximum likelihood estimation procedure, the actual parameter identification problem reads as:

$$\hat{\mathbf{p}} = \arg\min_{\mathbf{p}} \sum_{k=1}^{K} ||\mathbf{y}^{\mathrm{data}}(t_k) - \mathbf{y}(t_k, \mathbf{p})||_2^2, \tag{22}$$

where $||\cdot||_2$ denotes the Euclidean norm, and the model output equation is defined as:

$$\mathbf{y}(t_k, \mathbf{p}) = \mathbf{g}(\mathbf{x_d}(t_k, \mathbf{p})), \tag{23}$$

with $\mathbf{g} : \mathbf{R}^{x_d} \to \mathbf{R}^{n_y}$. Due to additive measurement noise and the Doob–Dynkin lemma (Rao and Swift, 2006), the identified model parameters $\hat{\mathbf{p}}$ can be considered to be random variables, where the probability space $(\Omega, \mathcal{F}, P)$ is defined with the sample space Ω, the σ-algebra $\mathcal{F}$, and the probability measure P. Precise parameter estimates necessitate, in addition to the high data quality (e.g., low measurement noise), high parameter sensitivities. Consequently, the MBDoE and the GSA-MBDoE aim to maximize parameter sensitivities.

3.2 Parameter Sensitivities

In the literature, local sensitivities are the standard in the MBDoE (Turanyi, 1990; Scire Jr. et al., 2001; Saltelli et al., 2005). Local sensitivities $S^l(\mathbf{p})$ are given as:

$$S^l[j,i](t) = \left.\frac{\partial \mathbf{y}[j](t)}{\partial \mathbf{p}[i]}\right|_{\hat{\mathbf{p}}}, \tag{24}$$

where $S^l(\mathbf{p}) \in \mathbf{R}^{n_y \times n_p}$, and $\hat{\mathbf{p}}$ is the latest update of the estimated model parameter vector. Note that local parameter sensitivities $S^l(\mathbf{p})$ are an essential component of the FIM and the MBDoE (Walter and Pronzato, 1997; Pukelsheim, 2006).

Alternatively, GSA treats the model parameters, $\mathbf{p}$, and the model outcomes, $\mathbf{y}$, as random variables and aims to quantify the amount of variance that each parameter, $\mathbf{p}[i]$, contributes to the total variance of the jth model output, $\sigma^2(\mathbf{y}[j](t))$ (Saltelli et al., 2005). The conditional variance is given as $\underset{-i}{\sigma}^2(\mathbf{y}[j](t)|\mathbf{p}[i])$, and the subscript $-i$ indicates that the variance is taken over all parameters other than $\mathbf{p}[i]$. The expected value of the resulting conditional variance reads as $\underset{i}{E}\left[\underset{-i}{\sigma}^2(\mathbf{y}[j](t)|\mathbf{p}[i])\right]$, and the subscript notation of $\underset{i}{E}$ indicates that the expected value is taken only over the parameter $\mathbf{p}[i]$. The total output variance, $\sigma^2(\mathbf{y}[j](t))$, is split into two additive terms (Saltelli et al., 2005). With:

$$\sigma^2(\mathbf{y}[j](t)) = \underset{i}{\sigma}^2(\underset{-i}{E}[\mathbf{y}[j](t)|\mathbf{p}[i]]) + \underset{i}{E}[\underset{-i}{\sigma}^2(\mathbf{y}[j](t)|\mathbf{p}[i])], \tag{25}$$

the global parameter sensitivities (a.k.a. first-order Sobol' indices) are defined as:

$$S^g[j,i](t) = \frac{\underset{i}{\sigma}^2(\underset{-i}{E}[\mathbf{y}[j](t)|\mathbf{p}[i]])}{\sigma^2(\mathbf{y}[j](t))}, \tag{26}$$

where $S^g(\mathbf{p}) \in \mathbf{R}^{n_y \times n_p}$, and $\sum_{i=1}^{n_p} S^g[j,i](t) \leq 1, \forall j \in \{1,\dots,n_y\}$.

3.3 Point Estimate Method

To avoid a computational overload when solving the dynamic optimization problem, the Sobol' indices have to be calculated efficiently. The PEM has proven beneficial in various engineering problems (Lerner, 2002), including complex (bio)chemical and electrochemical processes (Schenkendorf et al., 2018; Laue et al., 2019). Starting with a nominal parameter vector $\mathbf{p}_0$, dedicated model parameter vector realizations $\mathbf{p}_k$ form a parameter vector set, $\mathbf{p}_k \in \mathcal{O} := \{\mathbf{p}_0, \mathcal{O}_1, -\mathcal{O}_1, \mathcal{O}_2, -\mathcal{O}_2, \mathcal{O}_3, -\mathcal{O}_3\}$, where:

$$\mathcal{O}_1 := \{\mathbf{p}_0[i] + \vartheta,\ \forall i \in \{1,\dots,n_p\}\},$$
$$\mathcal{O}_2 := \{\mathbf{p}_0[(i,j)] + [+\vartheta, +\vartheta],\ \forall i, \underset{j>i}{j} \in \{1,\dots,n_p\}\},$$
$$\mathcal{O}_3 := \{\mathbf{p}_0[(i,j)] + [-\vartheta, +\vartheta],\ \forall i, \underset{j>i}{j} \in \{1,\dots,n_p\}\}.$$

The overall parameter sample number, n_{PEM}, scales quadratically with the dimension of uncertain model parameters:

$$n_{PEM} = 2n_p^2 + 1. \tag{28}$$

Based on the parameter samples $\mathbf{p}_k$, statistics of the output functions can be approximated. For instance, the expected value, $\mathbf{E}[\cdot]$, of the output is defined as:

$$\mathbf{E}[\mathbf{y}(\mathbf{p})] \approx \sum_{k=1}^{n_{PEM}} w_k \mathbf{y}(\mathbf{p}_k), \tag{29}$$

where, assuming a standard Gaussian distribution, the permutation parameter and weight factors are $\vartheta = \sqrt{3}, w_0 = 1 + \frac{n_p^2 - 7n_p}{18}, w_{1,\dots,2n_p+1} = \frac{4-n_p}{18}, w_{2n_p+2,\dots,n_{PEM}} = \frac{1}{36}$. Note that any parametric or non-parametric probability distribution of relevant model parameters can be considered via a (non)linear transformation step, including parameter correlations (Xie et al., 2018).

Next, the variance, $\sigma^2[\cdot]$, can be estimated with the following equation:

$$\sigma^2[\mathbf{y}(\mathbf{p})] \approx \sum_{k=1}^{n_{PEM}} w_k (\mathbf{y}(\mathbf{p}_k) - \mathbf{E}[\mathbf{y}(\mathbf{p})])^2. \tag{30}$$

Note that due to a nested re-sampling strategy, the global sensitivity matrix (Eq. (26)) can be determined highly efficiently with n_{PEM} model simulations, where appropriate subsets, $\mathcal{P}_i \subset \mathcal{O}$, are evaluated to calculate $S^g(\mathbf{p}[i])$, $\forall i \in \{1,\dots,n_p\}$. For more details regarding the PEM in GSA and robust process design, please refer to Schenkendorf et al. (2018).

To rate the efficiency of the GSA-MBDoE, the following efficiency measure is used:

$$\eta = \sigma_l^2[\hat{\mathbf{p}}] / \sigma_g^2[\hat{\mathbf{p}}], \tag{31}$$

where the uncertainty in the estimated model parameters, $\hat{\mathbf{p}}$, is quantified with empirical statistics:

$$\sigma_{l/g}^2[\hat{\mathbf{p}}] \approx \sum_{k=1}^{n_{MC}} \frac{1}{n_{MC}-1} (\hat{\mathbf{p}}_k - \mathbf{E}[\hat{\mathbf{p}}])^2. \tag{32}$$

Here, n_{MC} Monte Carlo simulations with artificial data assuming additive white measurement noise are used.

4. CASE STUDY

To demonstrate the effectiveness of the proposed GSA-MBDoE concept (Eq. (26)), optimal experimental operating conditions for the SPMeT (Eqs. (1)-(23)) are calculated and compared with the outcome of the standard MBDoE based on local parameter sensitivities (Eq. (24)). In particular, we optimize an experiment with a fixed duration time, $t_{exp} = 1000\,\text{s}$. The optimal input sequence is considered to be piece-wise constant over each 100 s resulting in a control variable vector of $n_v = 10$ elements. Each element is limited to $[\mathbf{u}[i]_{min}, \mathbf{u}[i]_{max}] = [-15\,\text{C}, 15\,\text{C}]$, with $i = 1, \cdots, n_v$. The measurement sampling time of the correspondent voltage and temperature is $t_s = 5s$; i.e., $\mathbf{y}(t_k) = [V(t_k); T(t_k)]$. Note that considering a measurements sampling time which is independent from the number of control variables enables to adapt the DoE to the time constants of different processes. The same initial conditions x_0 are used for all MBDoE results: the positive stoichiometry is initialized as 0.83 (which corresponds to a SOC of 5%), and the initial temperature is set equal to 298.15 K, while the initial electrolyte concentration and the average concentration flux are assumed to start at equilibrium values of $1000\,\text{mol/m}^3$ and zero, respectively. The experiments should not exceed temperature and voltage limits ($T(t_k) \leq 320\,\text{K}$ and $2.7\,\text{V} \leq V(t_k) \leq 4.2\,\text{V}$), which are taken into account by the soft constraint in (21d). For the sake of simplicity, nine normalized performance-relevant model parameters are studied, and the parameter vector reads as $\mathbf{p} = [De^0, E_{a,D_{p,s}}, k_p^0, k_n^0, E_{a,k_p}, E_{a,k_n}, \tau_s, \tau_n, h_c]$. Note that the information of all nominal model parameters can be found in Ecker et al. (2015b,a). When considering nine model parameters, the overall sample number needed to calculate the global parameter sensitivity matrix, S^g, reads as $n_{PEM} = 163$. Note that for GSA, a standard deviation of 10% is assumed for these nine model parameters. In this study, the so-called *D-criteria* (Walter and Pronzato, 1997) is implemented as a cost function:

$$\Phi(S^{l/g}(\mathbf{p})) = det(S^{l/g}(\mathbf{p})^T S^{l/g}(\mathbf{p})), \tag{33}$$

where $F(\mathbf{p}) := S^l(\mathbf{p})^T S^l(\mathbf{p})$ can be considered as the FIM.

Technically, the resulting optimization problem (Eq. (21)) was solved by using the interior point NLP solver IPOPT, where a multi-start strategy was used to avoid local minima. In Fig. 1, we show the optimized current input profiles obtained with the MBDoE and the GSA-MBDoE. The profiles in the first interval, $t \leq 500\,\text{s}$, show different trends. Both start with the high negative current input, but only GSA-MBDoE switches to the high positive current input afterward. In the second interval, $t > 500\,\text{s}$, the resulting current profiles show a *bang-bang* control behavior, that is, switching from the high negative current input to the high positive current input and back.

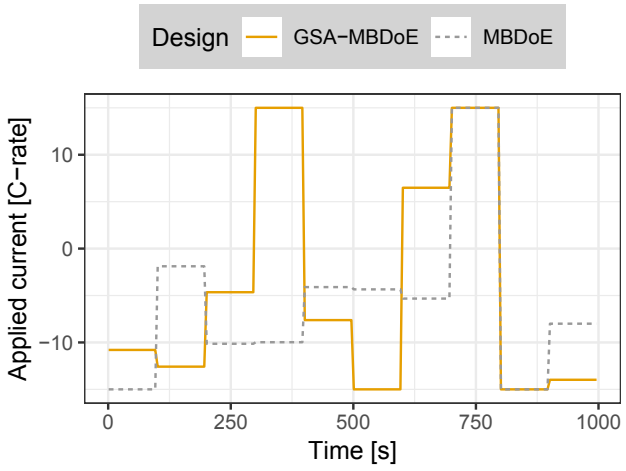

Fig. 1. Current input profiles based on the MBDoE (local approach) and the GSA-MBDoE (global approach).

The performance of the MBDoE and GSA-MBDoE designs is validated with Monte Carlo simulations (Eq. (32)), that is, 100 simulated experimental data sets with additive white noise ($\sigma_y^2(V) = 10^{-2}, \sigma_y^2(T) = 0.3$) are used for the parameter identification step. Based on the parameter estimates (Eq. (22)) and the resulting parameter uncertainties (Eq. (32)) the efficiency of the GSA-MBDoE (Eq. 31), is given in Table 1. The efficiency measure, η, clearly shows an improvement of the GSA-MBDoE result compared to the MBDoE outcome. For all parameters, the GSA-MBDoE ensures more precise parameter estimates, that is, the optimized current input profile based on the GSA-MBDoE generates more informative data than the MBDoE did. Note that the measurement sample numbers for the GSA-MBDoE and MBDoE design are identical. The model parameter uncertainties of k_n^0 and E_{a,k_n} are reduced significantly, and the parameter τ_s is marginally affected by a particular current input profile. In Fig. 2, we study the resulting parameter uncertainties in more detail. In the lower-left triangle, the scatter plots of all parameter combinations are given. The MBDoE results in stronger parameter variations and outliers in comparison with the GSA-MBDoE; see k_n^0 and E_{a,k_n} results. In the case of τ_s, two sample clusters can be detected, indicating two local minima of the parameter identification problem, which is insensitive to the GSA-MBDoE or MBDoE setting. On the diagonal, we illustrate the corresponding box-and-whisker plots. Obviously, the GSA-MBDoE-based parameter estimates are more precise and have fewer outliers. Based on the illustrated median and spread, only a few parameters might have a Gaussian probability density function, as in Fig. 3a for E_{a,k_n}. In most cases, the probability density functions are non-Gaussian or non-symmetric, which is common for non-linear identification problems. For instance, the probability density function of τ_s is bimodal and has two peaks, because of the two local minima of the parameter identification problem; see Fig. 3b. The probability density function of τ_n, in turn, shows a significant skewness in its estimates; see Fig. 3c. In the upper-right triangle of Fig. 2, the parameter correlations are shown. The GSA-MBDoE does not guarantee the lowest parameter correlation for all parameter combinations. Note, however, that parameter correlations

Table 1. GSA-MBDoE efficiency according to Eq. (31).

Parameter	De^0	$E_{a,D_{p,s}}$	k_p^0	k_n^0	E_{a,k_p}
Efficiency η	1.3970	2.2971	1.9015	17.6513	1.7172

Parameter	E_{a,k_n}	τ_s	τ_n	h_c
Efficiency η	3.2228	1.0050	1.8365	1.6938

were not included in the cost function when using the *D-criteria*, but could be considered explicitly with dedicated anti-correlation criteria.

5. CONCLUSIONS

The usefulness of model-based concepts in advanced battery management systems depends critically on the quality of the model parameters. In this work, we successfully demonstrated that a model-based experimental design, which evaluates global parameter sensitivities (GSA-MBDoE) instead of local parameter sensitivities (MBDoE), ensures informative data and more precise parameter estimates, respectively. As a case study, the single-particle model with electrolyte and thermal dynamics (SPMeT) was implemented, and optimal current profiles were identified. Moreover, the point estimate method (PEM) ensured low computational costs of the proposed GSA-MBDoE concept. In the case of non-globally identifiable parameter identification problems, e.g., a parameter with several local minima, optimal experimental design concepts have to be advanced with rigorous parameter identifiability measures. Moreover, novel ideas of a fast global sensitivity analysis are needed if we have to study the impact of more model parameters or if we want to solve more complex optimization problems, e.g., a higher dimension of the control input vector or additional degrees of freedom of the experimental design.

REFERENCES

Bizeray, A.M., Kim, J.H., Duncan, S.R., and Howey, D.A. (2018). Identifiability and parameter estimation of the single particle lithium-ion battery model. *IEEE Transactions on Control Systems Technology*, 27(5), 1862–1877.

Chaturvedi, N.A., Klein, R., Christensen, J., Ahmed, J., and Kojic, A. (2010). Algorithms for advanced battery-management systems. *IEEE Control Systems*, 30(3), 49–68.

Chu, Y. and Hahn, J. (2013). Necessary condition for applying experimental design criteria to global sensitivity analysis results. *Computers & Chemical Engineering*, 48, 280–292.

Di Domenico, D., Stefanopoulou, A., and Fiengo, G. (2010). Lithium-ion battery state of charge and critical surface charge estimation using an electrochemical model-based extended Kalman filter. *Journal of Dynamic Systems, Measurement, and Control*, 132(6), 061302.

Doyle, M., Fuller, T.F., and Newman, J. (1993). Modeling of galvanostatic charge and discharge of the lithium/polymer/insertion cell. *Journal of the Electrochemical Society*, 140(6), 1526–1533.

Ecker, M., Käbitz, S., Laresgoiti, I., and Sauer, D.U. (2015a). Parameterization of a physico-chemical model

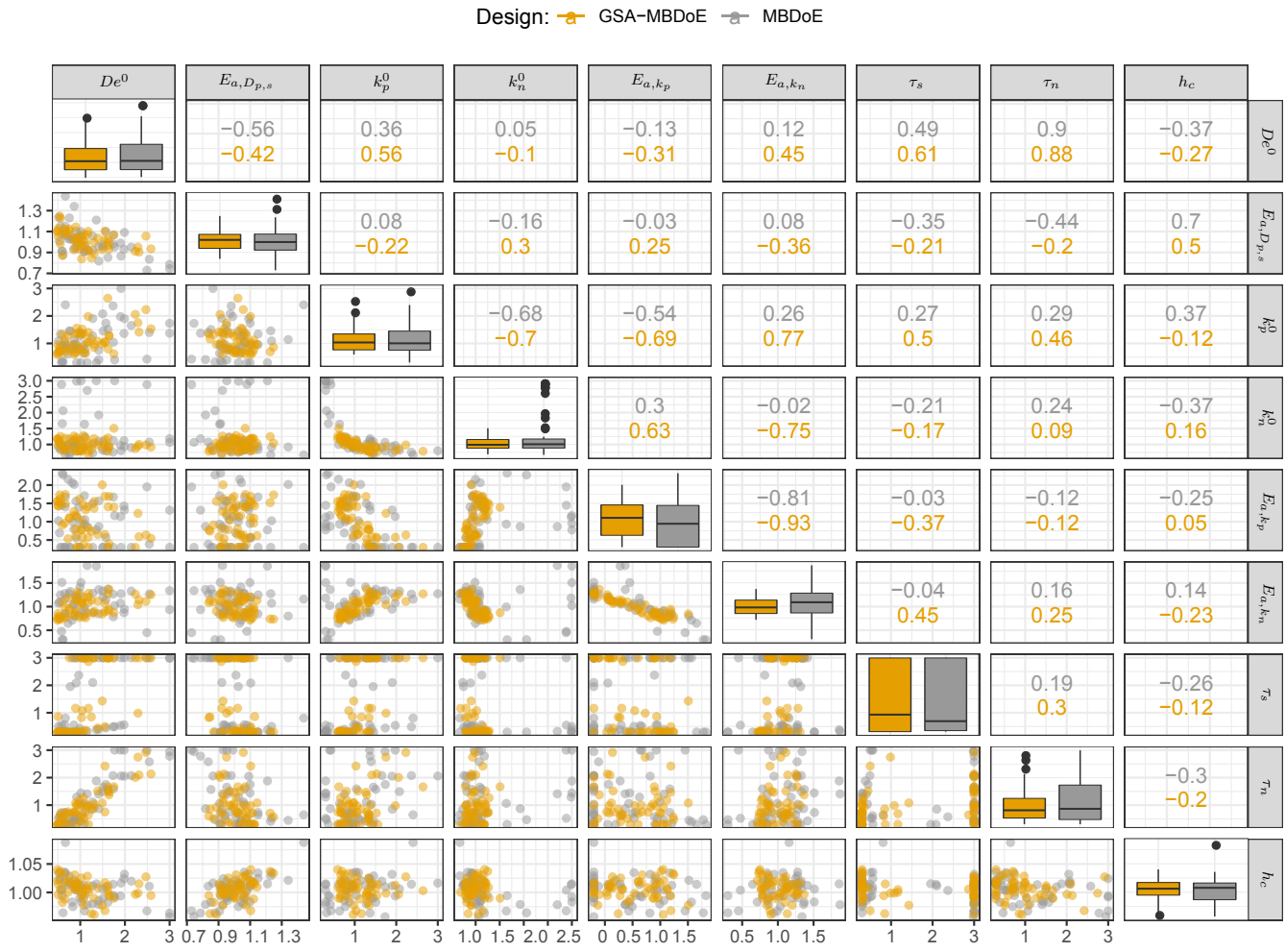

Fig. 2. Statistics of the parameter estimates for the MBDoE and the GSA-MBDoE: scatter plots of all parameter combinations (lower-left triangle), corresponding box-and-whisker plots (diagonal), and parameter correlations (upper-right triangle).

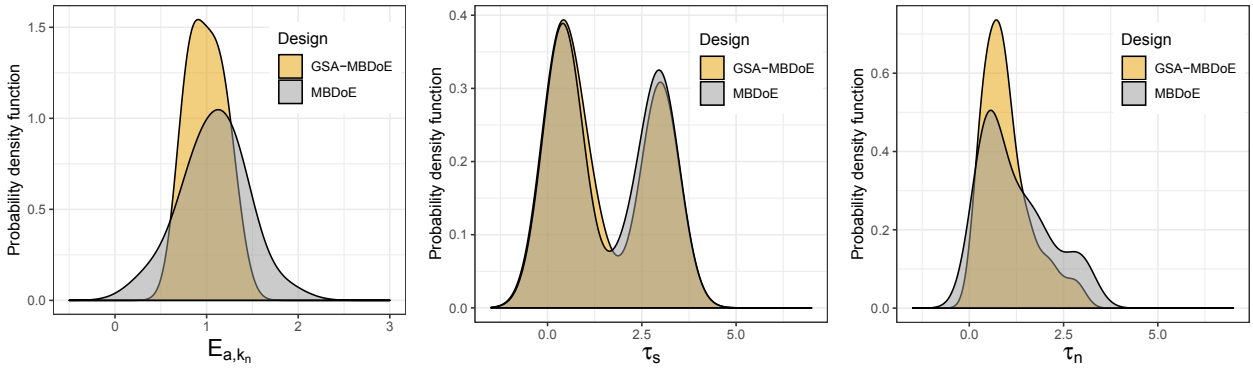

(a) Gaussian **(b)** Bimodal **(c)** Non-symmetric

Fig. 3. Resulting probability density functions of the estimated parameters based on the MBDoE and the GSA-MBDoE show: (a) Gaussian, (b) bimodal, and (c) non-symmetric distributions.

of a lithium-ion battery II. Model validation. *Journal of The Electrochemical Society*, 162(9), A1849–A1857.

Ecker, M., Tran, T.K.D., Dechent, P., Käbitz, S., Warnecke, A., and Sauer, D.U. (2015b). Parameterization of a physico-chemical model of a lithium-ion battery I. Determination of parameters. *Journal of The Electrochemical Society*, 162(9), A1836–A1848.

Forman, J.C., Moura, S.J., Stein, J.L., and Fathy, H.K. (2012). Genetic identification and fisher identifiability analysis of the doyle–fuller–newman model from experimental cycling of a lifepo4 cell. *Journal of Power Sources*, 210, 263–275.

Gomadam, P.M., Weidner, J.W., Dougal, R.A., and White, R.E. (2002). Mathematical modeling of lithium-ion and nickel battery systems. 110(2), 267–284.

Hu, X., Li, S., and Peng, H. (2012). A comparative study of equivalent circuit models for li-ion batteries. *Journal of Power Sources*, 198, 359–367.

Kiefer, J. (1959). Optimum experimental designs. *Journal of the Royal Statistical Society. Series B (Methodological)*, 21(2), 272–319.

Laue, V., Schmidt, O., Dreger, H., Xie, X., Röder, F., Schenkendorf, R., Kwade, A., and Krewer, U. (2019). Model-Based Uncertainty Quantification for the Product Properties of Lithium-Ion Batteries. *Energy Technology*, 1900201.

Lerner, U.N. (2002). Hybrid bayesian networks for reasoning about complex systems. Technical report.

Manesso, E., Sridharan, S., and Gunawan, R. (2017). Multi-objective optimization of experiments using curvature and fisher information matrix. *Processes*, 5(4).

Mendoza, S., Rothenberger, M., Hake, A., and Fathy, H. (2016). Optimization and experimental validation of a thermal cycle that maximizes entropy coefficient fisher identifiability for lithium iron phosphate cells. *J. Power Sources*, 308, 18–28.

Mendoza, S., Rothenberger, M., Liu, J., and Fathy, H.K. (2017). Maximizing parameter identifiability of a combined thermal and electrochemical battery model via periodic current input optimization. *IFAC PapersOnLine*, 50(1), 7314–7320.

Moura, S.J. (2015). Estimation and control of battery electrochemistry models: A tutorial. In *2015 54th IEEE Conference on Decision and Control (CDC)*, 3906–3912. IEEE.

Moura, S.J., Argomedo, F.B., Klein, R., Mirtabatabaei, A., and Krstic, M. (2017). Battery state estimation for a single particle model with electrolyte dynamics. *IEEE Transactions on Control Systems Technology*, 25(2), 453–468.

Ning, G. and Popov, B.N. (2004). Cycle life modeling of lithium-ion batteries. *Journal of The Electrochemical Society*, 151(10), A1584–A1591.

Park, S., Kato, D., Gima, Z., Klein, R., and Moura, S. (2018a). Optimal experimental design for parameterization of an electrochemical lithium-ion battery model. *Journal of The Electrochemical Society*, 165(7), A1309–A1323.

Park, S., Kato, D., Gima, Z., Klein, R., and Moura, S. (2018b). Optimal input design for parameter identification in an electrochemical li-ion battery model. In *2018 Annual American Control Conference (ACC)*, 2300–2305. IEEE.

Perez, H.E., Hu, X., and Moura, S.J. (2016). Optimal charging of batteries via a single particle model with electrolyte and thermal dynamics. 4000–4005.

Perez, H.E., Hu, X., Dey, S., and Moura, S.J. (2017). Optimal charging of Li-ion batteries with coupled electro-thermal-aging dynamics. *IEEE Transactions on Vehicular Technology*, 66(9), 7761–7770.

Pozzi, A., Ciaramella, G., Gopalakrishnan, K., Volkwein, S., and Raimondo, D.M. (2018a). Optimal design of experiment for parameter estimation of a single particle model for lithiumion batteries. In *2018 IEEE Conference on Decision and Control (CDC)*, 6482–6487. IEEE.

Pozzi, A., Ciaramella, G., Volkwein, S., and Raimondo, D.M. (2018b). Optimal design of experiments for a lithium-ion cell: Parameters identification of an isothermal single particle model with electrolyte dynamics. *Industrial & Engineering Chemistry Research*, 58(3), 1286–1299.

Pukelsheim, F. (2006). *Optimal design of experiments*. SIAM.

Rao, M.M. and Swift, R.J. (2006). *Probability theory with applications*. Springer.

Rodriguez-Fernandez, M., Kucherenko, S., Pantelides, C., and Shah, N. (2007). Optimal experimental design based on global sensitivity analysis. *Computer Aided Chemical Engineering*, 24, 63 – 68.

Saltelli, A., Ratto, M., Tarantola, S., and Campolongo, F. (2005). Sensitivity analysis for chemical Models. *Chemical Reviews*, 105, 2811–2828.

Santhanagopalan, S., Guo, Q., Ramadass, P., and White, R.E. (2006). Review of models for predicting the cycling performance of lithium ion batteries. *Journal of Power Sources*, 156(2), 620–628.

Schenkendorf, R., Xie, X., Rehbein, M., Scholl, S., and Krewer, U. (2018). The Impact of Global Sensitivities and Design Measures in Model-Based Optimal Experimental Design. *Processes*, 6(4), 27.

Scire Jr., J., Dryer, F., and Yetter, R. (2001). Comparison of global and local sensitivity techniques for rate constants determined using complex reaction mechanisms. *International Journal of Chemical Kinetics*, 33(12), 784–802.

Sinkoe, A. and Hahn, J. (2017). Optimal experimental design for parameter estimation of an il-6 signaling model. *Processes*, 5(3).

Subramanian, V.R., Diwakar, V.D., and Tapriyal, D. (2005). Efficient macro-micro scale coupled modeling of batteries. *Journal of The Electrochemical Society*, 152(10), A2002–A2008.

Torchio, M., Magni, L., Gopaluni, R.B., Braatz, R.D., and Raimondo, D.M. (2016). Lionsimba: A matlab framework based on a finite volume model suitable for Li-ion battery design, simulation, and control. *Journal of The Electrochemical Society*, 163(7), A1192–A1205.

Turanyi, T. (1990). Sensitivity Analysis of Complex Kinetic Systems. Tools and Applications. *Journal of Mathematical Chemistry*, 5, 203–248.

Walter, E.E. and Pronzato, L. (1997). *Identification of parametric models from experimental data*. Springer.

Xie, X., Krewer, U., and Schenkendorf, R. (2018). Robust optimization of dynamical systems with correlated random variables using the point estimate method. *IFAC-PapersOnLine*, 51(2), 427–432.

Zou, C., Manzie, C., and Anwar, S. (2014). Control-oriented modeling of a lithium-ion battery for fast charging. *IFAC Proceedings Volumes*, 47(3), 3912–3917.